Influence of the Long-Chain/Short-Chain Amphiphile Ratio on Lateral Diffusion of PEG-Lipid in Magnetically Aligned Lipid Bilayers as Measured via Pulsed-Field-Gradient NMR

Ronald Soong and Peter M. Macdonald
Department of Chemistry, University of Toronto, and Department of Chemical and Physical Sciences, University of Toronto at Mississauga, Canada

ABSTRACT Lateral diffusion measurements of polyethylene glycol(PEG)-lipid incorporated into magnetically aligned lipid bilayers, composed of dimyristoyl phosphatidylcholine (DMPC) plus dihexanoyl phosphatidylcholine (DHPC) plus 1 mol % (relative to DMPC) dimyristoyl phosphatidylethanolamine-*n*-[methoxy(polyethylene glycol)-2000] (DMPE-PEG 2000), were performed using stimulated-echo pulsed-field-gradient proton (^{1}H) nuclear magnetic resonance spectroscopy. The DMPE-PEG 2000 (1 mol %, 35°C) lateral diffusion coefficient D varied directly with the mole fraction of DMPC, $X_{DMPC} = q/(1 + q)$ where q = DMPC/DHPC molar ratio, decreasing progressively from $D = 1.65 \times 10^{-11}$ m^2 s^{-1} at $q \approx 4.7$ to $D = 0.65 \times 10^{-11}$ m^2 s^{-1} at $q \approx 2.5$. Possible sources of this dependence, including orientational disorder, obstruction, and PEG-lipid sequestration, were simulated using, respectively, a diffusion-in-a-cone model, percolation theory, and a two-phase PEG distribution model. Orientational disorder alone was not capable of reproducing the observations, but in combination with either obstruction or PEG-lipid two-phase distribution models did so satisfactorily. A combination of all three models yielded the most reasonable fit to the observed dependence of lateral diffusion on q. These same effects would be expected to influence lateral diffusion of any bilayer-associating species in such systems.

INTRODUCTION

Lateral diffusion of bilayer membrane components is fundamental to membrane function, and lateral diffusion measurements provide a valuable perspective on membrane structure and lateral organization (1–5). The most widely and successfully employed technique for determining membrane lateral diffusion coefficients involves fluorescence-recovery-after-photobleaching (FRAP) measurements on fluorophore-tagged membrane-bound diffusants (2,3).

To avoid FRAP's requirement for an attached fluorophore with its attendant synthetic challenges and concerns regarding perturbation, nuclear magnetic resonance techniques have been developed for measuring lateral diffusion coefficients in bilayer membranes. One such technique, described recently, uses pulsed-field-gradient (PFG) nuclear magnetic resonance (NMR) spectroscopy to measure membrane lateral diffusion coefficients in magnetically aligned lipid bilayers (6). In PFG NMR a pulsed linear gradient of magnetic field is imposed across the sample such that the nuclear spin resonance frequency becomes transiently position dependent (7). The experiment is arranged such that refocusing of the nuclear-spin magnetization in an echo-type sequence decreases with increasing translational diffusion in the direction of the applied field gradient. The PFG NMR method is well established in studies of molecular diffusion in both isotropic and anisotropic media (for reviews, see 8–11), and has been applied to study lateral diffusion in lipid bilayers either under magic-angle spinning conditions (12), or macroscopically aligned between glass slides oriented at the magic-angle (13,14), both of which situations produce narrow resonance lines.

Bicelles, or bilayered micelles, also yield narrow NMR resonances by virtue of their tendency to spontaneously align in magnetic fields. They consist of mixtures of long chain and short chain amphiphiles which self-assemble such that the long-chain amphiphiles form a planar lipid bilayer whereas the short-chain amphiphiles segregate to regions of high curvature at the edges of the bilayer (for reviews, see 15–17). When placed in a magnetic field, bicelles composed of mixtures of dimyristoyl phosphatidylcholine (DMPC) with dihexanoyl phosphatidylcholine (DHPC), first introduced by Sanders and Schwonek (18), spontaneously align such that the normal to the plane of the lipid bilayer is oriented perpendicular to the direction of the magnetic field (19). It has been demonstrated that PFG ^{1}H NMR on magnetically aligned bicelles, in the case of a magnetic field gradient oriented perpendicular to the direction of bicellar alignment, directly measures lateral diffusion within the plane of the bicelle's lipid bilayer (6).

Despite their wide popularity in NMR studies, critical details of bicelle morphology remain controversial. The classical view holds that bicelles consist of planar disks having DMPC sequestered to the planar bilayer disk body with DHPC sequestered to the highly-curved disk edges (15). Although there is general agreement that this disk morphology pertains at temperatures below the DMPC phase-transition temperature and at low lipid concentrations and low DMPC/DHPC ratios, where the bicelles are small and free to tumble isotropically, at higher lipid concentrations

Submitted April 15, 2005, and accepted for publication June 17, 2005.

Address reprint requests to P. M. Macdonald, Tel.: 905-828-3805; E-mail: pmacdona@utm.utoronto.ca.

0006-3495/05/09/1850/11 $2.00

doi: 10.1529/biophysj.105.064725

and/or higher DMPC/DHPC ratios small-angle neutron scattering (SANS) studies indicate a conversion to a morphology consisting of DMPC-rich continuous bilayer lamellae perforated by toroidal holes lined with DHPC (20,21). This view has received support from fluorescence-resonance-energy-transfer studies (22), but remains controversial (23,24).

PFG NMR lateral diffusion measurements of bicelle-incorporated polyethylene glycol (PEG)-lipids indicate that, for DMPC/DHPC = 4.5 bicelles, PEG-lipids experience unrestricted lateral diffusion over diffusion distances on the order of microns, a finding that supports the perforated lamellae model rather than the disk model of bicelle morphology (6). PEG-lipids are added to bicelles to enhance bicelle stability by virtue of steric stabilization (25). They consist of a hydrophobic anchoring group, such as dimyristoyl phosphatidylethanolamine (DMPE), to which a PEG group is covalently attached through the lipid's polar headgroup. The water-soluble PEG becomes effectively grafted to the lipid bilayer surface through its DMPE hydrophobic anchor. Lateral diffusion of PEG-lipid is particularly facile to measure using PFG ^{1}H NMR because the PEG headgroup is highly mobile and provides a narrow NMR resonance.

The ratio of long-chain to short-chain amphiphiles in the bicelle mixture is a critical determinant of bicelle morphology. To date, its influence on lateral diffusion within bicelles has not been investigated, but one anticipates several possible mechanisms through which such influence might be exerted. In particular, if there is a morphological change from a perforated lamellar to a discoidal phase, then lateral diffusion will become restricted by the dimensions of the disks. Further, regardless of the morphological phase, bicelle orientational order decreases with decreasing DMPC/DHPC ratio (15), an effect likely to decrease the apparent lateral diffusion coefficient. Moreover, any DHPC-rich toroidal perforations, the number and/or size of which depend on the DMPC/DHPC ratio, will act as obstructions to lateral diffusion. Finally, PEG-lipids partition between highly curved and planar regions of bicelles (26–28), where their diffusion properties should differ markedly—resulting in an altered PEG-lipid lateral diffusion with increasing DHPC content.

Ultimately, it is desired to develop bicelles as a general platform for lateral diffusion measurements of not just PEG-lipid, but any amphiphilic membrane-associating species whether protein, or lipid, or drug. Consequently, we have undertaken PFG ^{1}H NMR measurements of the lateral diffusion of PEG-lipids in magnetically aligned DMPC plus DHPC bicelles as a function of the ratio q = DMPC/DHPC to examine the influence of this critical parameter, to better understand bicelle morphology, and to potentiate measurements on a wider range of diffusants.

EXPERIMENTAL MATERIALS

1,2-dimyristoyl-*sn*-glycero-3-phosphocholine (DMPC), 1,2-dihexanoyl-*sn*-glycero-3-phosphocholine (DHPC), and 1,2-dimyristoyl-*sn*-glycero-3-phosphoethanolamine-*n*-methoxy(polyethylene glycol)-2000 (DMPE-PEG 2000) were purchased from Avanti Polar Lipids (Alabaster, AL). All other biochemicals and reagents were purchased from Sigma-Aldrich (Oakville, ON).

Sample preparation

Bicelles were prepared to consist of either 15 wt % or 25 wt % lipid in aqueous 150 mM NaCl + 50 mM Tris-HCl, ph 7.4, in D_2O, as described previously (29,30). The ratio q, being the proportion of long-to-short chain amphiphiles (DMPC/DHPC), was varied between $\sim q = 2.4$ and $q = 4.7$, with the exact value in any one sample being determined via ^{31}P NMR spectroscopy. DMPE-PEG 2000 was included in all bicelle preparations at the level of 1 mol % relative to DMPC.

NMR spectroscopy

All NMR spectra were recorded on a Chemagnetics (Fort Collins, CO) CMX300 NMR spectrometer using a magnetic resonance imaging/spectroscopy probe (Doty Scientific, Columbia, SC) equipped with actively shielded gradient coils and dual radio-frequency channels in addition to the lock channel. Note that the various NMR spectra of the magnetically aligned samples investigated here consist of relatively narrow resonances spread over relatively narrow spectral ranges and, as such, may be acquired under conditions usual to solution-state NMR spectroscopy. Details regarding the spectral referencing, acquisition, and processing conditions for ^{2}H, ^{31}P, and ^{1}H NMR spectra are provided elsewhere (6). All spectra were recorded at a sample temperature of 35°C ± 0.5°C.

^{1}H NMR diffusion measurements were performed using the pulsed-field gradient (PFG) stimulated-echo (STE) procedure (31), with phase cycling of the radio frequency pulses to remove unwanted echoes (32), and a train of gradient pulses to equalize eddy current effects (33), as described previously (6). The gradient strength (typically 250 G cm^{-1}) was calibrated from the known diffusion coefficient of HDO at 25°C (34).

RESULTS AND DISCUSSION

The STE PFG NMR method for bilayer lateral diffusion measurements relies on spontaneous magnetic orientation to produce macroscopically aligned bilayers. To demonstrate that such macroscopic alignment has been achieved, Fig. 1 shows ^{2}H NMR (Fig. 1 *A*) and ^{31}P NMR spectra (Fig. 1 *B*) of 25 wt % lipid magnetically aligned DMPC/DHPC ($q = 4.7$) bilayers containing 1 mol % DMPE-PEG 2000, all obtained at 35°C.

Spectrum *A* is a ^{2}H NMR spectrum of HDO and exhibits a quadrupolar splitting equal, here, to 44 Hz, in agreement with previous reports (19,35,36). The residual quadrupolar splitting arises from fast exchange of HDO between bulk water and oriented water bound at the surface of magnetically aligned lipid bilayers.

Spectrum *B* in Fig. 1 is a ^{31}P NMR spectrum of the same magnetically aligned bilayers and shows two narrow well-resolved resonances. The more intense upfield resonance occurs at −12.45 ppm (referenced to 85% H_3PO_4), a frequency indicative of liquid-crystalline DMPC contained within a magnetically aligned bilayer oriented with its bilayer normal perpendicular to the direction of the magnetic field (15). The second resonance occurs at −5.33 ppm and has an integrated intensity of $\sim 1/(4.7 \pm 0.2)$ relative to that

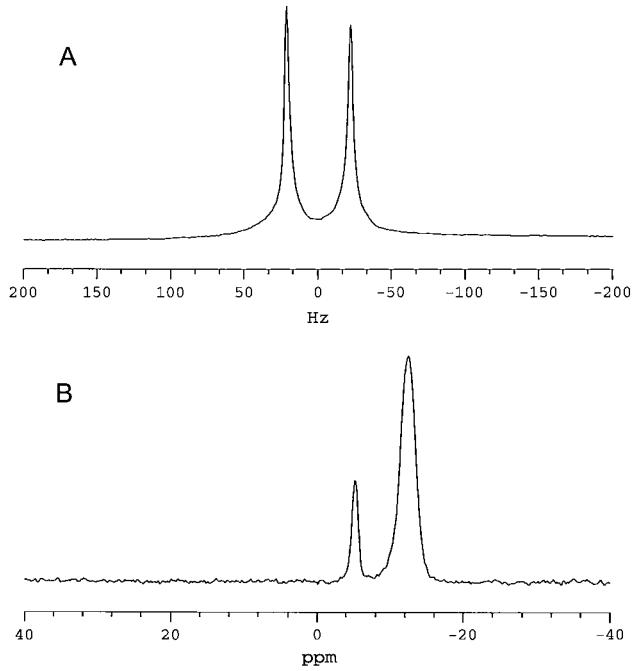

FIGURE 1 NMR spectra (35°C) of magnetically aligned bilayers: DMPC/DHPC (q = 4.7, 25 wt % lipid) + 1 mol % DMPE-PEG 2000. (*A*) ^{2}H NMR spectrum of HDO. The residual quadrupolar splitting of 44 Hz indicates magnetic alignment of bilayers. (*B*) ^{31}P NMR spectrum showing resonances from DMPC (−12.45 ppm) and DHPC (−5.33 ppm), DMPC/DHPC intensity ratio of 4.7 ± 0.2. The position of the DMPC resonance is indicative of bilayers aligned with their normal to the plane of the bilayer oriented perpendicular to the direction of the magnetic field. The resonance from 1 mol % DMPE-PEG 2000 is not resolved.

at −12.45 ppm, indicating that it arises from DHPC. (The signal/noise ratios of the DMPC and DHPC resonances were 60 and 30, respectively, equating to a 5% error in the determination of q through this method.) The smaller residual chemical shift anisotropy of DHPC relative to DMPC is a consequence of the former's tendency to segregate into regions of high local curvature. The ^{31}P NMR spectra confirm, therefore, that magnetic alignment of the bilayers has been achieved, and that the alignment of the bilayer normal is perpendicular to the magnetic field direction. The ^{31}P NMR resonance due to 1 mol % DMPE-PEG 2000 is too small to discern in such spectra.

Fig. 2 illustrates the effects of varying q on the ^{31}P NMR residual chemical shift anisotropy of DMPC and DHPC, where we convert to the less commonly used but more transparent variable of the mole fraction of DMPC, $X_{\mathrm{DMPC}} = q/(1 + q)$. There is a general trend toward lower values of these anisotropic quantities with decreasing X_{DMPC}, as expected given that q scales the system order. For the case of chemical shift anisotropy one may quantify the order parameter S_{bilayer} as described by Sanders et al. (15),

$$S_{\mathrm{bilayer}} = \frac{\delta_{\mathrm{obs}} - \delta_{\mathrm{iso}}}{\delta_{90} - \delta_{\mathrm{iso}}}, \qquad (1)$$

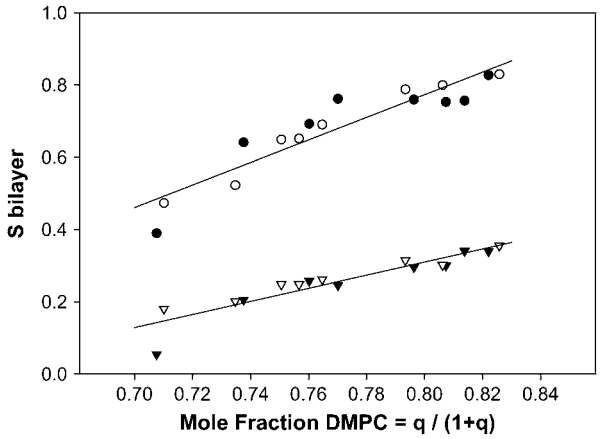

FIGURE 2 Bilayer orientational order as a function of the mole fraction of DMPC. S_{bilayer} was calculated from the ^{31}P NMR chemical shift as per Eq. 1 in the text. The mole fraction of DMPC was calculated using $X_{\mathrm{DMPC}} = q/(1 + q)$ where q was derived from the relative integrated intensities of the ^{31}P NMR resonances of DMPC versus DHPC. Circles, DMPC; triangles, DHPC. Open symbols, 25 wt % lipid; solid symbols, 15 wt % lipid. The straight lines show linear regression fits to the combined 15 and 25 wt % lipid data. For DMPC the regression line has slope 3.13, intercept −1.73, and r^2 0.87. For DHPC the regression line has slope 1.81, intercept −1.14, and r^2 0.86.

where δ_{obs} is the observed ^{31}P NMR chemical shift of the perpendicular aligned bilayers relative to the isotropic chemical shift δ_{iso}, whereas δ_{90} is the chemical shift of the 90°, i.e., upfield, shoulder in the ^{31}P NMR powder spectrum of corresponding nonoriented bilayers. S_{bilayer}, then, quantifies the degree to which the instantaneous symmetry axis of the bilayers deviates from the idealized average orientation of 90° relative to the magnetic field direction. The ^{31}P NMR data for DMPC and DHPC are expressed in this fashion in Fig. 2, and confirm the trend toward decreasing bilayer order with increasing DHPC, in accord, both qualitatively and quantitatively, with earlier observations (15). Within the limits of the scatter of the data, the relationship between S_{bilayer} and X_{DMPC} is approximately linear. No consistent difference was discernible between samples containing 15 wt % and 25 wt % lipid.

Fig. 3 shows a series of ^{1}H NMR spectra from $q = 4.7$ (25 wt % lipid, 35°C) mixtures containing 1 mol % DMPE-PEG 2000 as a function of increasing gradient-pulse duration δ in the stimulated-echo (STE) pulsed-field-gradient (PFG) NMR pulse sequence (31), employed here for measurement of lateral diffusion coefficients. The two dominant resonances are those of HDO (4.2 ppm) and the overlapping resonances of the DHPC choline methyl protons (3.2 ppm) and the PEG ethylene oxide protons (3.3 ppm). The rationale for this assignment has been described previously (6). The broad ^{1}H NMR resonances expected from the acyl chain, glycerol backbone, or headgroup protons of DMPC (37,38), all of which experience significant residual homonuclear dipolar interactions, are largely absent with an echo delay time of

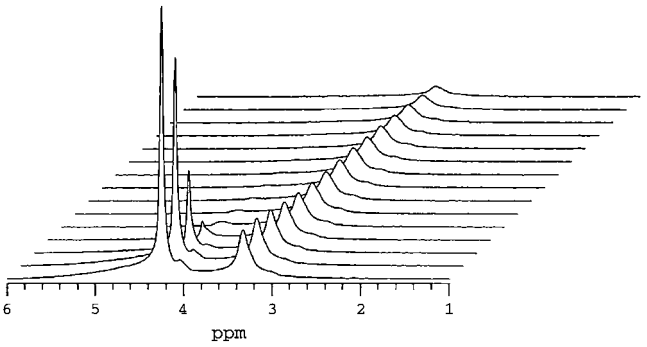

FIGURE 3 ^{1}H NMR spectra (35°C) of magnetically aligned DMPC/DHPC ($q = 4.7$, 25 wt % lipid) + 1 mol % DMPE-PEG 2000 bilayers as a function of the field-gradient-pulse duration δ in the STE PFG NMR sequence. The two major resonances are assigned to HDO (4.2 ppm) and overlapping DPME-PEG 2000 ethoxy and DHPC choline methyl protons (3.3 ppm). Other lipid resonances are not visible due to their short transverse relaxation times relative to the spin-echo delay (10 ms) used in the acquisition of this spectrum. The gradient-pulse amplitude was 250 G cm^{-1}, whereas τ_2 equaled 10 ms and τ_1 equaled 200 ms. Gradient pulse durations were, from front to back in units of ms, 0.1, 0.25, 0.50, 0.75, 1.0, 1.25, 1.5, 1.75, 2.0 2.5, 3.0, 3.5, 4.0, 5.0, and 6.0. The water resonance at 4.2 ppm decays rapidly due to water's fast diffusion. The combined DHPC choline methyl and DMPE-PEG 2000 headgroup resonance at 3.3 ppm decays far more slowly, as expected for bilayer intercalated species.

10 ms due to rapid transverse relaxation. The PEG headgroup and the DHPC choline methyls, in contrast, experience nearly isotropic motional freedom due to, respectively, rapid rotational isomerization within the ethylene oxides of the PEG headgroup and rapid exchange of DHPC on and off the bilayers. Thus, these resonances are ideally narrow for our STE PFG NMR lateral diffusion measurements.

In STE PFG NMR diffusion measurements, center-of-mass diffusion causes the intensity of the stimulated echo to decay according to Eq. 2,

$$I = I_0 \exp\left(\frac{-2\tau_2}{T_2}\right)\exp\left(\frac{-\tau_1}{T_1}\right)\exp[-D(\gamma g\delta)^2(\Delta - \delta/3)], \tag{2}$$

where D is the isotropic diffusion coefficient, γ is the relevant magnetogyric ratio, g is the gradient pulse amplitude, δ is the gradient pulse duration, $\Delta = \tau_1 + \tau_2$ is the experimental diffusion time, and T_1 and T_2 are the longitudinal and transverse relaxation times, respectively. The gradient pulses are applied during the interpulse delays τ_2 to encode and then decode a given diffusing species according to its chemical shift and any change of position along the gradient direction. During the interpulse delay τ_1, the nuclear spin magnetization is stored along the z-direction so that, for situations where $T_1 > T_2$, the experimentally accessible diffusion time $\Delta = \tau_1 + \tau_2$ is limited by T_1 rather than T_2. In this way the STE PFG NMR sequence may permit the use of longer diffusion times, thereby facilitating diffusion measurements for cases of slower diffusion, or lower gradient strengths, or lower γ nuclei. Experimentally, either the gradient-pulse amplitude, or its duration, or the diffusion time, is incremented progressively and the diffusion coefficient is extracted from the slope in a plot of $\mathrm{Ln}(I/I_0)$ versus $(\gamma g\delta)^2(\Delta - \delta/3)$.

The series of ^{1}H NMR spectra shown in Fig. 3 were acquired as a function of increasing gradient-pulse duration δ with a gradient strength of 250 G cm^{-1}, whereas $\tau_1 = 200$ ms and $\tau_2 = 10$ ms. Of the two dominant resonances, the HDO resonance intensity decays almost immediately to invisibility with increasing δ, due to water's rapid diffusion and the particular choices of gradient strength and delays τ_1 and τ_2. Using Eq. 2 to fit the decay of the proton resonance of HDO in this sample yields a water diffusion coefficient equal to 1.6×10^{-9} m^2 s^{-1}. This is roughly a factor-of-two slower water diffusion in oriented bilayers relative to bulk water at the same temperature (34), the difference being attributed to the large fraction of bilayer surface-bound water in fast exchange with the bulk. Since in our measurements the field gradient was applied in a single direction only, perpendicular to the bilayer normal of the aligned bilayers, it is not possible to observe the anisotropy of water diffusion known to occur in macroscopically oriented bilayers in general (39) and in magnetically aligned bicelles in particular (40,41).

In Fig. 3 the combined [DHPC choline methyl + PEG headgroup] resonance decays far more slowly than that of the water, as expected for lipids constrained to diffuse laterally within a bilayer. Importantly, the particular choices of diffusion time $\Delta = 210$ ms and gradient strength $g = 250$ G cm^{-1} produce a substantial decay of the resonance intensity over an accessible range of gradient-pulse durations δ, sufficient to measure reliably the lipid's lateral diffusion coefficient.

Lateral diffusion in membranes is inherently anisotropic, so that for field gradients applied solely along the laboratory z-direction, as is the case here, only the D_{zz} element of the diffusion tensor is measured (7). After transforming into a molecular frame defined with respect to the lipid bilayer, only two independent diffusion tensor elements persist: specifically, $D_{||}$ and $D\perp$ representing, respectively, diffusion parallel and perpendicular to the bilayer normal (13,42). Thus, $D\perp$ corresponds to lateral diffusion within the bilayer. For the case of macroscopically aligned lipid bilayers in the presence of a field gradient applied parallel to the direction of the main magnetic field, g_z, the measured diffusion coefficient becomes

$$D = D_\perp \sin^2\theta + D_\parallel \cos^2\theta, \tag{3}$$

where θ is the polar angle between the bilayer normal and the direction of the applied field gradient.

It is reasonable to assume that diffusion parallel to the bilayer normal is orders-of-magnitude slower than diffusion perpendicular to the bilayer normal, i.e., lateral diffusion, so the second term in Eq. 3 may be ignored. For spontaneously magnetically aligned DMPC/DHPC bilayers, the bilayer normal is oriented at 90° relative to the magnetic field

direction. Hence for a perfectly aligned bilayer sample, i.e., having an infinitely narrow mosaic spread of alignments, the apparent diffusion coefficient measured in our STE PFG NMR experiment is directly equal to the lateral diffusion coefficient within the bilayer.

For the case of well-resolved resonances, knowledge of T_1 or T_2 is not essential to diffusion coefficient measurements via the STE PFG NMR technique since typically both τ_1 and τ_2 are constant in any one measurement series. For the case of overlapping or poorly-resolved resonances, however, the echo intensity in the STE PFG NMR experiment is a sum of contributions, and knowledge of the individual T_1 and T_2 relaxation times is a prerequisite to extracting the individual diffusion coefficients from the overall intensity decay.

Table 1 lists values of T_1 and T_2 measured for the combined [DMPE-PEG 2000 headgroup + DHPC choline methyl] resonance in magnetically aligned bilayers at 35°C. The overlapping DHPC choline methyl and PEG resonances have individual T_1 and T_2 relaxation times that are too similar to permit a resolution of their individual contributions to either T_1 inversion recoveries or T_2 spin-echo intensity decays. Hence, a weighted average value of T_1 and T_2 is reported. In all cases $T_1 > T_2$ by at least an order of magnitude, confirming that the STE PFG NMR sequence is an optimal choice for diffusion measurements in these cases. Although there is significant scatter across the range of sample compositions, in general both T_1 and T_2 are shorter for the 25 wt % lipid than for the 15 wt % lipid samples. Although no consistent dependence of T_1 on q is evident, it appears that lower values of q yield somewhat longer values of T_2.

TABLE 1 ^{1}H NMR Longitudinal (T_1) and transverse (T_2) relaxation times for combined [DMPE-PEG 2000 headgroup + DHPC choline methyl] resonance in magnetically aligned bilayers at 35°C

				T_2¶ (ms)	
q = DMPC/DPHC*	X_{DHPC}†	X_{PEG}‡	T_1§ (ms)	PEG	DHPC
15 wt % lipid					
2.4	0.60	0.40	733	41	15
3.2	0.54	0.46	734	31	23
2.8	0.57	0.43	731	25	15
3.4	0.53	0.47	850	33	29
3.9	0.50	0.50	773	34	27
4.2	0.49	0.51	791	31	28
4.4	0.48	0.52	763	25	20
4.6	0.47	0.53	668	21	21
25 wt % lipid					
2.5	0.59	0.41	668	27	10
2.8	0.57	0.43	684	24	11
3.1	0.55	0.45	707	19	11
3.0	0.55	0.45	687	18	12
3.3	0.54	0.46	716	18	11
3.8	0.51	0.49	695	15	11
4.2	0.49	0.51	695	14	10
4.7	0.47	0.53	680	14	13

*Determined from the relative integrated intensities of the respective ^{31}P NMR resonances.

†The fractional contribution of the nine DHPC choline methyl protons relative to the 1 mol % DMPE-PEG 2000 headgroup protons for the experimentally determined q.

‡The fractional contribution of the 1 mol % DMPE-PEG 2000 headgroup protons, based on four protons per 45 ethylene oxide units per DMPE-PEG 2000, relative to the DHPC choline methyl protons at the experimentally determined q.

§The intensities of the combined [DHPC choline methyls + DMPE-PEG 2000 headgroup] proton resonance in the inversion-recovery experiment could not be resolved into separate contributions and were fit as a single exponential having the indicated T_1.

¶The intensities of the combined [DHPC choline methyls + DMPE-PEG 2000 headgroup] proton resonance in the spin-echo experiment could not be resolved into separately decaying contributions and were fit to a single exponential having the indicated PEG T_2. However, in fitting the diffusion decays according to Eq. 4, better fits were obtained by adjusting the DHPC T_2 to the shorter value indicated in the table.

The diffusion coefficient is derived from a plot of Ln (I/I_0) versus $(\gamma g\delta)^2(\Delta-\delta/3)$ as shown in Fig. 4. For a population undergoing unrestricted center-of-mass diffusion characterized by a single uniform diffusion coefficient, such a plot should be linear with a slope proportional to the diffusion coefficient. This is clearly not the case for the combined [DHPC choline quaternary methyl + PEG headgroup] resonance. As reported previously (6), the best description of the observed diffusion decay assumes a superposition of decays from two diffusing species, one being DHPC and the other being DMPE-PEG 2000, according to Eq. 4,

$$I/I_0 = X_{DHPC}\exp\left(\frac{-2\tau_2}{T_{2DHPC}}\right)\exp\left(\frac{-\tau_1}{T_{1DHPC}}\right)\exp(-kD_{DHPC}) + X_{PEG}\exp\left(\frac{-2\tau_2}{T_{2PEG}}\right)\exp\left(\frac{-\tau_1}{T_{1PEG}}\right)\exp(-kD_{PEG}), \quad (4)$$

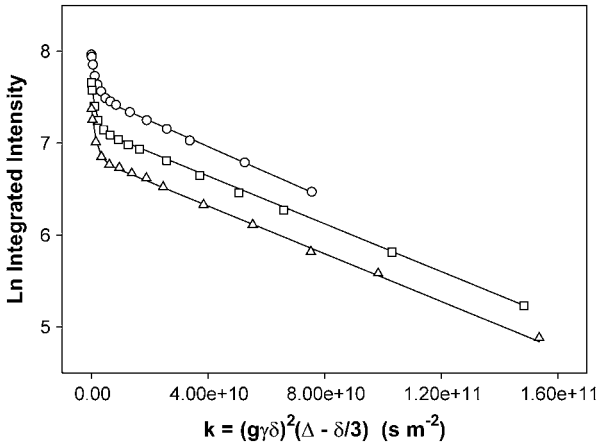

FIGURE 4 Normalized stimulated-echo intensity decays from STE PFG ^{1}H NMR spectra (35°C) of magnetically aligned DMPC/DHPC (q = 4.7, 25 wt % lipid) bilayers + 1 mol % DMPE-PEG 2000. Gradient amplitude = 250 G cm^{-1}. Circles, Δ = 210 ms; squares, Δ = 410 ms; and triangles, Δ = 610 ms. Lines of best fit using Eq. 4 are shown with $D_{DHPC} = 7.0 \times 10^{-10}$ m^2 s^{-1}, values of X_{DHPC}, X_{PEG}, T_1, and T_2 as per Table 1, and $D = 1.40 \times 10^{-11}$ m^2 s^{-1} at Δ = 210 ms, whereas $D = 1.3 \times 10^{-11}$ m^2 s^{-1} at both Δ = 410 ms and Δ = 610 ms.

where $k = [(\gamma g \delta)^2(\Delta - \delta/3)]$, and $X_{DHPC} = 1 - X_{PEG}$ is the fractional intensity contributed initially by the DHPC choline quaternary methyl protons, and D_{DHPC} and D_{PEG} are the diffusion coefficients of DHPC and DMPE-PEG 2000, respectively. In fitting diffusion data of the type shown in Fig. 4 to Eq. 4, it is assumed that all of the DHPC choline quaternary methyl and the PEG headgroup protons are initially NMR-visible, with intensities modulated by their respective T_1 and T_2 relaxation times. Optimal fits were obtained when $T_{2\ DHPC}$ was permitted to vary somewhat, while $T_{2\ PEG}$ was held fixed at the value listed in Table 1. Values of $T_{2\ DHPC}$ yielding optimal fits were generally somewhat shorter, as listed in Table 1. D_{DHPC} values were always $\sim 7.0 \times 10^{-10}$ m^2 s^{-1}, in agreement with previous measurements for $q = 4.5$ bilayers at 25 wt % lipid in water and 35°C (6). The particular choice of $T_{2\ DHPC}$ and D_{DHPC}, in fact, has only a marginal influence on the remaining fitting quantity, D_{PEG}, since this is determined primarily from the slope of the intensity decay at larger k-values where the intensity contributed by DHPC is minimal due to its faster diffusion. Specifically, for $q = 4.7$ bilayers containing 1 wt % DMPE-PEG 2000 at 25 wt % lipid and 35°C, D_{PEG} is found to equal 1.40×10^{-11} m^2 s^{-1} in the case $\Delta = 210$ ms, which lies in the range expected for a diacyl phospholipid diffusing laterally within the plane of a liquid-crystalline lipid bilayer (3).

The series of three STE PFG NMR intensity decays in Fig. 4 were obtained for the combined [DHPC choline quaternary methyl + DMPE-PEG 2000 headgroup] resonance for three different values of the diffusion time $\Delta = \tau_1 + \tau_2$ wherein τ_2 was held constant at 10 ms while τ_1 was altered progressively from 200 to 400 to 600 ms. The intensity decay is progressively greater with increasing Δ due to the combined effects of T_1 relaxation and longer diffusion time. The curves of best fit shown in the figure were obtained using Eq. 4, employing the known values of X_{PEG} and X_{DHPC}, values of T_1 and T_2 for the DHPC choline methyl and the DMPE-PEG 2000 headgroup protons as per Table 1, allowing D_{DHPC} to equal 7.0×10^{-10} m^2 s^{-1}, and inputting D_{PEG} as the parameter of fit for the three different diffusion times. It is found that with increasing diffusion time Δ, the observed DMPE-PEG 2000 diffusion coefficient decreased only slightly from 1.40×10^{-11} m^2 s^{-1} at $\Delta = 210$ ms, to 1.3×10^{-11} m^2 s^{-1} at both $\Delta = 410$ ms and $\Delta = 610$ ms. All three diffusion coefficients fall within the range expected for liquid-crystalline lipids (3).

For all values of q investigated here, the DMPE-PEG 2000 diffusive decays in plots of the type shown in Fig. 4 were linear with increasing δ and the DMPE-PEG 2000 diffusion coefficient was nearly independent of the diffusion time Δ. This indicates that over the range $2.4 < q < 4.7$ investigated here, these mixtures retain a perforated lamellar morphology, because the planar regions of this phase form a continuous phase permitting unrestricted lateral diffusion over large distances. Specifically, for two-dimensional diffusion, the root-mean-square (RMS) lateral diffusion distance is calculated according to Eq. 5,

$$\langle r^2 \rangle^{1/2} = [4Dt]^{1/2}, \quad (5)$$

where D is the diffusion coefficient and $t = \Delta$ is the characteristic experimental diffusion time. For DMPE-PEG 2000 in magnetically aligned bilayers, where typically $D = 1.60 \times 10^{-11}$ m^2 s^{-1} and for $\Delta = 615$ ms, the RMS diffusion distance of DMPE-PEG 2000 equals 6.27 μm. The radius of an ideal discoidal bicelle may be calculated for a given q (43) and equals 300 Å for the case $q = 4.5$, decreasing progressively with decreasing q. Since the experimental RMS lateral diffusion distance far exceeds the size of a single discoidal bicelle, and no evidence of restricted diffusion is apparent (restricted diffusion would produce a flattening of the diffusive decays in Fig. 4 at larger values of k), our results demonstrate that the perforated lamellar phase is maintained over this range of q, temperature, and wt % lipid. Note that this morphology is not unique to DMPC/DHPC mixtures. Perforated, or defective, lamellar phases in fact have been observed in a number of different amphiphilic self-assemblies, and can be shown to align in magnetic fields (Ref. 44 and references therein).

Fig. 5 compares the DMPE-PEG 2000 diffusion coefficients derived from STE PFG ^{1}H NMR intensity decays for magnetically aligned bicelles at both 15 wt % and 25 wt % lipid, as a function of the mole fraction of DMPC, X_{DMPC}. There is evidently a progressive decrease in diffusion coefficient with decreasing DMPC content (increasing DHPC). The diffusion coefficients at 25 wt % lipid were consistently smaller than those at 15 wt % lipid.

If there is no morphological change from the perforated lamellar phase over the range of q investigated here, then

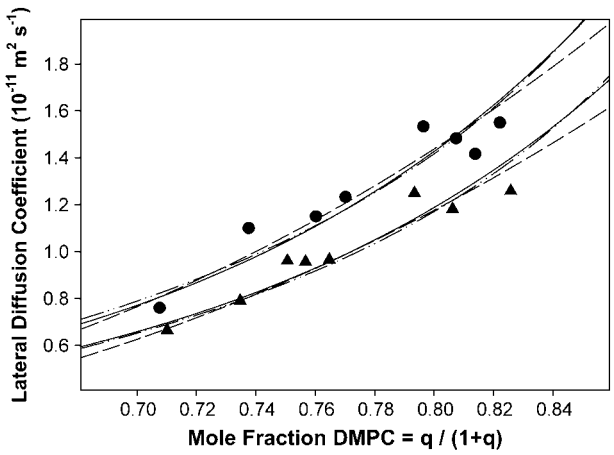

FIGURE 5 The STE PFG ^{1}H NMR derived lateral diffusion coefficient of DMPE-PEG 2000 in DMPC/DHPC magnetically aligned bilayers (35°C) as a function of the mole fraction of DMPC. Values plotted are the mean of diffusion coefficients obtained at $\Delta = 210$, 410, and 610 ms. Triangles, 25 wt % lipid; and circles, 15 wt % lipid. The solid curves are fits to the diffusion data obtained using a combination of orientational disorder, obstruction, and two-phase PEG distribution models as described in the text: order × obstruction, dashed line; order × two-phase, dashed-dotted-dotted line; and order × obstruction × two-phase, solid line.

other sources of the influence of the bilayer DMPC/DHPC ratio q on the lateral diffusion coefficient of DMPE-PEG 2000 in magnetically aligned bilayers as measured by STE PFG ^{1}H NMR need to be examined. Several likely possibilities can be envisioned. First, since decreasing the ratio q also decreases the bilayer orientational ordering (15), it may be that D is linked to S_{bilayer}. Second, assuming the perforated lamellar phase applies, decreasing q must increase the surface coverage of toroidal holes, thereby progressively obstructing lateral diffusion. Third, PEG-lipid may distribute between curved and planar regions of the bicelle (26–28), and may experience different lateral diffusion behavior in each, the effect obviously scaling proportionately with q. The focus of the remainder of this article will be to address which, if any, of these possibilities appears reasonable.

Bilayer orientational order and lateral diffusion

To address the relationship between the apparent diffusion coefficient, D_{app}, and the magnetically aligned bilayer's orientational order, S_{bilayer}, we invoke the diffusion-in-a-cone model (45–47) to describe fluctuations of the bilayer normal with respect to the magnetic field direction. We assume that such fluctuations occur in addition to those usually undergone by lipids in bilayer membranes as proposed by Sanders et al. (15) in their definition of S_{bilayer}. Such motions might consist of collective local fluctuations or undulations occurring with a rate that is fast relative to the measurement time. Hence, the $\sin^2\theta$ term in Eq. 3 must be replaced with its time- and ensemble-average value $\langle \sin^2\,\theta\rangle$ as per Eq. 6,

$$D_{\text{app}} = D_{\perp}\langle \sin^2\theta\rangle, \tag{6}$$

where θ is the angle between the bilayer normal and the direction of the magnetic field gradient. The diffusion-in-a-cone model as applied here assumes that the normal to the bilayer wobbles freely within a cone described by the cone semiangle β_0 and that the wobble is axially symmetric with respect to the azimuthal angle α as illustrated in Fig. 6. The orientational order parameter S_{bilayer} is then related to the cone semiangle β_0 as per Eq. 7 (45–47),

$$S_{\text{bilayer}} = \tfrac{1}{2}\cos\beta_0(1+\cos\beta_0). \tag{7}$$

To calculate $\langle \sin^2\theta\rangle$ we invoke ergodicity (time-average = number-average over ensemble), and assuming, further, a random distribution of bilayer normal vectors within the cone, we integrate over all values of θ, where $\cos\theta = \sin\beta\,\sin\alpha$ for the geometry in Fig. 6, resulting in Eq. 8,

$$\begin{aligned}\langle \sin^2\theta\rangle &= \frac{\int_0^{\beta_0}\int_0^{2\pi}(1-\sin^2\beta\sin^2\alpha)\sin\beta\,d\beta\,d\alpha}{\int_0^{\beta_0}\int_0^{2\pi}\sin\beta\,d\beta\,d\alpha}\\ &= 1-\frac{1}{3}\left[1-\frac{1}{2}\left(\frac{\cos\beta_0\sin^2\beta_0}{1-\cos\beta_0}\right)\right]\\ &= 1-\frac{1}{3}(1-S_{\text{bicelle}}).\end{aligned} \tag{8}$$

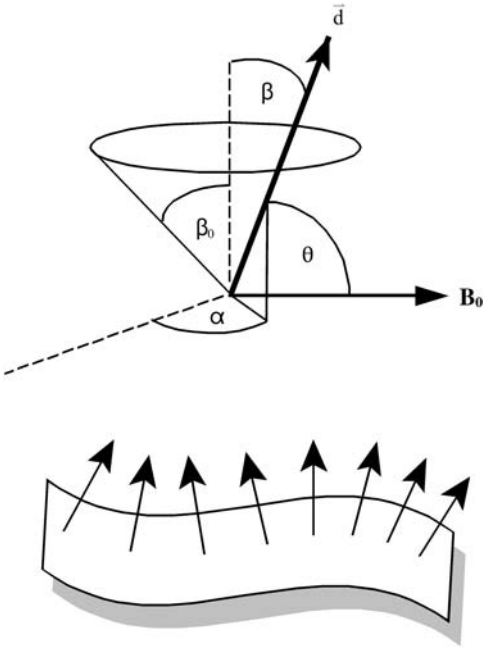

FIGURE 6 The diffusion-in-a-cone model as applicable to lateral diffusion measurements in magnetically aligned bilayers using STE PFG NMR measurements. Collective fluctuations of the bilayer normal d modulate the angle θ so that the ensemble- and time-average of $\langle \sin^2\,\theta\rangle$ enters Eq. 6. The normal is considered to diffuse freely in a cone of half-angle β_0, with its instantaneous orientation defined in terms of the polar-angle β and the azimuthal-angle α.

From Fig. 2, over the range $0.7 < X_{\text{DMPC}} < 0.8$ (i.e., $2.4 < q < 4.7$), S_{bilayer} decreases from ~0.80 to 0.40. Eq. 8 predicts, however, a decrease in the apparent diffusion coefficient on the order of only 14% over the same range of X_{DMPC}. Clearly the decrease in bilayer order alone is not sufficient to entirely explain the >50% reduction in the apparent diffusion coefficient of DMPE-PEG 2000 over the same range.

A further refinement of the diffusion-in-a-cone model is to assume a Gaussian distribution about the preferred orientation such that the order parameter is equated to the standard deviation of the Gaussian (45,48). Invoking such a Gaussian distribution, in fact, leads to predicted values of $\langle \sin^2\theta\rangle$ equally, or even more weakly, dependent on S_{bilayer} than those predicted by the constant distribution implicit in Eq. 8.

Toroidal obstruction and lateral diffusion

The DHPC-rich toroidal holes perforating the DMPC-rich lamellae should constitute obstructions to free diffusion. Obstruction effects increase in proportion to the surface area occluded by the obstruction, so that apparent diffusion should decrease with decreasing q-value, in qualitative agreement with our observations. To place this on a more quantitative footing we invoke the theoretical expression, Eq. 9, obtained by Van Beijeren and Kutner (49) for obstructed diffusion (where the relative diffusion coefficient $D^*(c,\gamma) = D(c,\gamma)/D(0)$ involves the diffusion coefficient $D(c,\gamma)$ at a concentration

c of obstacles of relative mobility γ, and $D(0)$ is the diffusion coefficient in the absence of obstacles),

$$D^*(c,\gamma) = (1-c)f(c,\gamma). \tag{9}$$

The correlation factor $f(c,\gamma)$ is

$$f(c,\gamma) = \frac{\left\{[(1-\gamma)(1-c)f_0 + c]^2 + 4\gamma(1-c)f_0^2\right\}^{1/2} - [(1-\gamma)(1-c)f_0 + c]}{2\gamma(1-c)f_0}, \tag{10}$$

$$f_0 = [1-\alpha]/[1+(2\gamma-1)\alpha], \tag{11}$$

where c is the area fraction of obstacles, γ is the ratio of the mobility of the observed diffusant relative to the obstacles, and α is a constant that depends on the lattice (e.g., square, triangular, or honeycomb).

Saxton (50) compared the results of Monte Carlo simulations of lateral diffusion with the behavior predicted by the theoretical expression of Van Beijeren and Kutner (49) and found generally good agreement. One exception was the situation in which the obstacles were completely immobile, where theory imperfectly predicted the percolation threshold. Another was at high surface coverage of obstacles, where generally there were small but significant discrepancies between theory and Monte Carlo simulation. For our purposes it is important to note that the Monte Carlo simulations of Saxton (50) indicate only a very weak dependence of the obstruction effect on the size of the obstacle, in contrast to the strong effect of the area fraction of obstacles.

To estimate the surface area fraction of toroidal holes c at a given q-value we assume first an idealized toroid as shown in Fig. 7. It is assumed further that DMPC occupies solely the planar regions whereas DHPC segregates exclusively to the curved edges. This annulus of DHPC has a radial thickness a, whereas the toroidal hole itself has a radius b. Assuming a uniform size of toroidal holes, the fractional surface area obstructed by toroids is

$$c = \frac{n_{\text{toroid}}A_{\text{toroid}}}{A_{\text{planar}} + n_{\text{toroid}}A_{\text{toroid}}}, \tag{12}$$

where n_{toroid} is the number of toroidal obstructions, and $A_{\text{toroid}} = \pi b^2$ ($b \geq a$ for all cases) is the surface area obstructed by each such toroid. The surface area of the inner toroidal annulus occupied by DHPC is

$$A_{\text{ring}} = 2\pi^2 ab - 4\pi a^2, \tag{13}$$

so that the number of DHPC per toroid becomes

$$n_{\text{DHPC}}^{\text{toroid}} = 2\pi^2\frac{ab}{d} - 4\pi\frac{a^2}{d}, \tag{14}$$

where d is the surface area occupied per DHPC, leading readily to the number of such toroids,

$$n_{\text{toroid}} = \frac{d\, n_{\text{DHPC}}^{\text{total}}}{2\pi^2 ab - 4\pi a^2}. \tag{15}$$

The planar area occupied by DMPC is simply the product of the number of DMPC and the area per DMPC. It is assumed that both DMPC and DHPC occupy identical surface areas d, since the phosphocholine headgroup is common to both. Substituting into Eq. 12, the fractional obstructed surface area becomes, simply,

$$c = [1 + q(\pi m - 2m^2)]^{-1}, \tag{16}$$

where $m = a/b$.

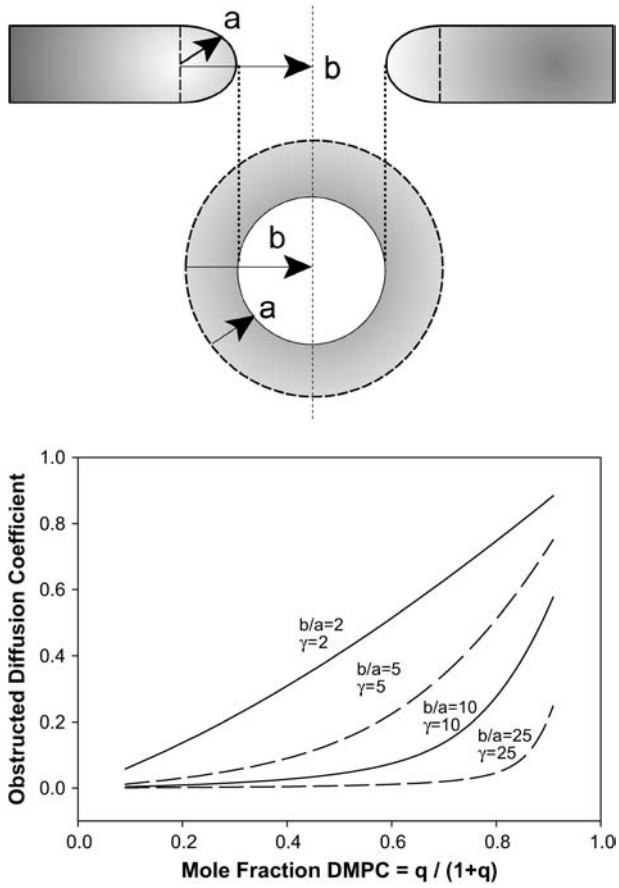

FIGURE 7 Obstruction effects for the perforated lamellae model of bicelle morphology and the predicted effects on PEG-lipid lateral diffusion. The perforated lamellae model posits the presence of DHPC-rich toroidal holes perforating the DMPC-rich bilayer lamella. In the schematic at the top, the toroidal holes are modeled in terms of an annulus of DHPC with radial dimension a and overall radius b, thereby permitting an evaluation of their fractional surface coverage as described in the text, in turn permitting an estimate of obstruction effects on lateral diffusion for a given mole fraction of DMPC and a particular mobility γ of the PEG-lipid relative to the toroidal hole. The graph shows the predicted apparent decrease in PEG-lipid lateral diffusion from such an obstruction model for various dimensions and mobilities of the toroidal holes as a function of the mole fraction of DMPC. Note that only relatively small, mobile holes yield lateral diffusion coefficients near those observed experimentally.

Calculation of the obstructed lateral diffusion coefficient $D^*(c,\gamma)$ requires an estimate of the size ratio $m = a/b$, where b is the radius of the toroidal holes, plus some estimate of the relative mobility γ of the tracer, i.e., DMPE-PEG 2000, versus the obstructions, i.e., the toroidal holes. Fig. 7 shows the predictions of this obstruction model for the lateral diffusion coefficient as a function of the mole fraction of DMPC for various sizes and mobilities of the toroidal obstructions. As expected, lateral diffusion decreases with increasing number of DHPC-rich toroidal holes, even when these are relatively small ($b/a = 2$) and mobile ($\gamma = 2$). The effect grows profoundly with increasing toroidal size and/or decreasing mobility. Thus, qualitatively, the obstruction model yields the desired dependence of lateral diffusion on the mole fraction of DMPC.

Quantitatively, provided that orientational disorder effects are included as per Eq. 8, the obstruction model provides a reasonable fit to both the 15 and 25 wt % lipid lateral diffusion data for the case $b/a = 5$ and $\gamma = 15$, using a value of $D(0)$ equal to 3.3×10^{-11} m^2 s^{-1} for 15 wt % and 2.7×10^{-11} m^2 s^{-1} for 25 wt% lipid, as shown via the dashed line in Fig. 5. The generally accepted hydrodynamic theory of Saffman and Delbrück (51) indicates only a weak logarithmic decrease in lateral diffusion with an increasing radius of diffusant. For instance, large membrane proteins such as the acetylcholine receptor, rhodopsin, and ATPase diffuse only approximately a factor of 2–3 times more slowly than DMPC (1). This suggests that $\gamma = 15$ represents unreasonably immobile toroidal holes. As for the size of the toroidal holes, we are not aware of any measurements of their dimension. However, the lateral diffusion coefficients measured here for DMPE PEG 2000 at higher values of q lie very close to those reported for 100% DMPC at comparable temperatures (52), indicating that obstruction effects are minimal at such q-values. This precludes the presence of large holes, since their obstruction effects already would be pronounced in the region $X_{DMPC} \approx 0.8$, and indicates that $b/a = 5$ is an acceptable choice for the size of the toroidal holes.

Two-phase PEG distribution model and lateral diffusion

Recent reports (26–28,53) strongly suggest that PEG-lipids accumulate in regions of high curvature, such as the annulus of lipids forming the toroidal holes of the perforated lamellae assumed to exist under the conditions pertinent to our DMPC/DHPC mixtures, as shown schematically in Fig. 8. Since lateral diffusion of any PEG-lipid contained within such a region would be restricted to that of the toroidal hole itself, this suggests that another explanation for the experimentally observed decrease in lateral diffusion of PEG-lipid with increasing mole fraction of DHPC is that PEG-lipid is in fast exchange between planar and highly curved regions of the bicelle assemblies. Slow exchange is precluded by the lack of any experimentally observed nonlinearity of diffusive decay of the PEG-lipid ^{1}H NMR signal (once DHPC diffusion is accounted for) or dependence on the diffusion time over the range 200 ms $< \Delta <$ 600 ms.

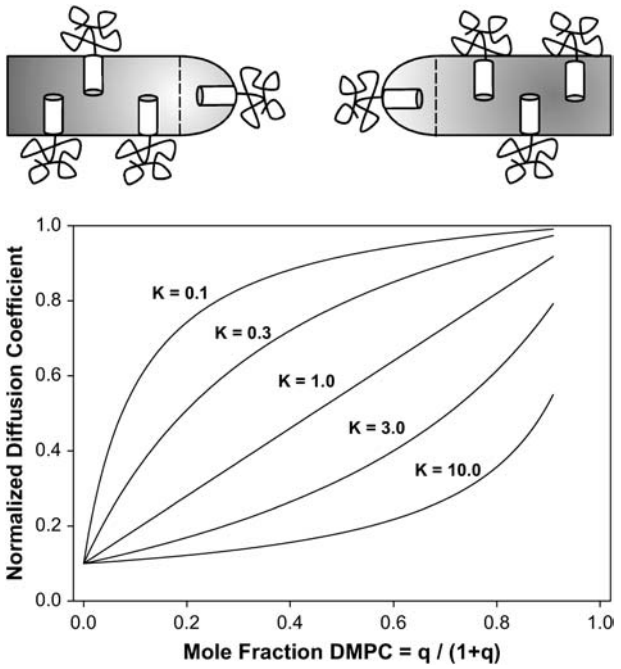

FIGURE 8 The two-phase PEG-lipid distribution model and its predicted effects on PEG-lipid lateral diffusion. PEG-lipid is considered to partition between planar and highly curved regions of the bilayers, as shown schematically at the top. Exchange between the two phases is fast on the NMR experimental diffusion timescale, whereas the partitioning is characterized by a partition constant K. Apparent diffusion along the direction of the applied field gradient (z-direction) is slow within the highly curved region because of geometric effects on $\sin^2\theta$. The graph shows the predicted apparent decrease in PEG-lipid lateral diffusion from such a two-phase PEG-distribution model for various values of the partition constant K, assuming that diffusion within the highly curved regions is a factor-of-10 slower than in the planar regions. Note that only values of K on the order of unity yield lateral diffusion coefficients near those observed experimentally.

In the case of fast exchange between two phases, the apparent diffusion coefficient equals

$$D_{APP} = X_A D_A + X_B D_B, \tag{17}$$

where X_i and D_i represent, respectively, the mole fraction and lateral diffusion coefficient of PEG-lipid in a particular phase (8). For a partition function $K = [B]/[A]$ describing the relative preference for one phase over another, the mole fraction in either phase equals

$$X_A = \left[\frac{1}{1+K}\times\frac{q}{1+q}\right]\left[\frac{1}{1+K}\times\frac{q}{1+q}+\frac{K}{1+K}\times\frac{1}{1+q}\right]^{-1}$$
$$X_B = \left[\frac{K}{1+K}\times\frac{1}{1+q}\right]\left[\frac{1}{1+K}\times\frac{q}{1+q}+\frac{K}{1+K}\times\frac{1}{1+q}\right]^{-1}, \tag{18}$$

where q = DMPC/DHPC, and phase A is equated with DMPC and phase B with DHPC.

Fig. 8 illustrates the apparent diffusion coefficient predicted by the two-phase PEG distribution model as a function of the

mole fraction of DMPC for various values of the partition function K, assuming a 10-fold slower lateral diffusion within the DHPC-rich toroidal holes relative to the DMPC-rich planar regions. Again, the behavior is similar qualitatively to that observed experimentally. Quantitatively, for both 15 and 25 wt % lipid data, only situations with K very large (e.g., 20, indicative of PEG-lipid heavily favoring the DHPC-rich phase) and D_B very slow (e.g., $0.0001 \times D_A$, indicative of virtually no diffusion of PEG-lipid within the DHPC-rich phase) reproduced the steep dependence of lateral diffusion on X_{DMPC}, as shown by the dashed-dotted line in Fig. 5, even when in combination with orientational order effects as per Eq. 8. Moreover, it was necessary to assume values of $D(0)$ equal to 9.2×10^{-11} m^2 s^{-1} for 15 wt % and 7.6×10^{-11} m^2 s^{-1} for 25 wt % lipid to achieve these fits. These, of course, are unreasonably high relative to literature values (52).

Combined orientational disorder, obstruction, and two-phase model

The three effects discussed here—orientational disorder, toroidal obstruction, and two-phase PEG distribution—should act in concert to influence the observed dependence of PEG-lipid lateral diffusion on X_{DMPC} in aligned bilayers. To predict their combined effects, the apparent diffusion coefficient in Eq. 17 is assumed to be an average over diffusion within two phases, where within the DMPC-rich planar region the diffusion coefficient of the PEG-lipid is reduced by obstruction, as predicted via Eqs. 9–16, and is scaled by orientational disorder effects, as per Eqs. 6–8. Such a combined model yields good fits to both the 15 and 25 wt % lipid diffusion data, as shown by the solid lines of fit in Fig. 5, using $b/a = 4$, $\gamma = 4$, $K = 4$, and $DB = 0.25$ for both, with values of the unperturbed diffusion coefficient $D(0)$ equal to 4.9×10^{-11} m^2 s^{-1} for 15 wt % lipid and 4.0×10^{-11} m^2 s^{-1} for 25 wt % lipid. These fitting parameters appear more physically reasonable than those obtained using the obstruction or distribution models alone.

CONCLUSIONS

Lateral diffusion of PEG-lipid in aligned bilayers is influenced by the ratio q of long-chain/short-chain amphiphiles composing the self-assembly. Smaller q equates to slower apparent lateral diffusion. Modeling indicates that this effect can be attributed to a combination of orientational disorder, obstruction by toroidal perforations, and the distribution of PEG-lipid between planar and highly curved phases. These same effects could be expected to influence the observed lateral diffusion of any bilayer-associating species, and unless caution were exercised might confound the analysis of other influences on lateral diffusion such as the presence of cholesterol, proteins, etc. Because the diffusive decays of our stimulated-echo amplitudes are strictly linear and virtually independent of the diffusion time it is not possible for us to differentiate definitively between the obstruction and the two-phase models. For instance, only near the percolation threshold will obstruction effects lead to a diffusion-time-dependent diffusion coefficient (50). But bicelles convert to an isotropic phase at $q \lesssim 2$, so the experiment cannot be performed. However, if the diffusion time can be shortened sufficiently that there is effectively slow exchange of PEG-lipid between the planar and the curved phases, then it may be possible to demonstrate directly the effects of the two-phase PEG-lipid distribution of lateral diffusion.

The authors thank Dr. Scott Prosser for his insightful comments.

This research was supported by a grant from the Natural Science and Engineering Research Council of Canada.

REFERENCES

1. Vaz, W. L. C., F. Goodsaid-Zaluondo, and K. Jacobson. 1984. Lateral diffusion of lipids and proteins in bilayer membranes. *FEBS Lett.* 174:199–207.
2. Jovin, T. M., and W. L. C. Vaz. 1989. Rotational and translational diffusion in membranes measured by fluorescence and phosphorescence methods. *Methods Enzymol.* 172:471–513.
3. Tocanne, J.-F., L. Dupou-Cézanne, and A. Lopez. 1994. Lateral diffusion of lipids in model and natural membranes. *Prog. Lipid Res.* 33:203–237.
4. Almeida, P. F. F., and W. L. C. Vaz. 1995. Lateral diffusion in membranes. *In* Handbook of Biological Physics. R. Lipovsky and E. Sackmann, editors. Elsevier, Amsterdam, The Netherlands. 305–357.
5. Saxton, M. J. 1999. Lateral diffusion of lipids and proteins. *Curr. Topics Membr.* 48:229–282.
6. Soong, R., and P. M. Macdonald. 2005. Lateral diffusion of PEG-lipid in magnetically aligned bicelles measured using stimulated echo pulse field gradient ^{1}H NMR. *Biophys. J.* 88:255–268.
7. Stejskal, E. O., and J. E. Tanner. 1965. Spin diffusion measurements—spin echoes in presence of a time-dependent field gradient. *J. Chem. Phys.* 42:288–295.
8. Stilbs, P. 1987. Fourier transform pulse-gradient spin-echo studies of molecular diffusion. *Progress NMR Spectrosc.* 19:1–45.
9. Kärger, J., H. Pfeifer, and W. Heink. 1988. Principles and applications of self-diffusion measurements by nuclear magnetic resonance. *Adv. Magn. Optic. Reson.* 12:1–89.
10. Price, W. S. 1997. Pulse-field gradient nuclear magnetic resonance as a tool for studying translational diffusion. I. Basic theory. *Concepts Magn. Reson.* 9:299–336.
11. Price, W. S. 1998. Pulse-field gradient nuclear magnetic resonance as a tool for studying translational diffusion. II. Experimental aspects. *Concepts Magn. Reson.* 10:197–237.
12. Gaede, H. C., and K. Gawrisch. 2004. Multi-dimensional pulsed field gradient magic angle spinning NMR experiments on membranes. *Magn. Reson. Chem.* 42:115–123.
13. Lindblom, G., and G. Orädd. 1994. NMR studies of translational diffusion in lyotropic liquid crystals and lipid membranes. *Progress NMR Spectrosc.* 26:483–515.
14. Orädd, G., and G. Lindblom. 2004. Lateral diffusion studied by pulsed field gradient NMR on oriented lipid membranes. *Magn. Reson. Chem.* 42:123–131.
15. Sanders, C. R., B. J. Hare, K. P. Howard, and J. H. Prestegard. 1994. Magnetically-oriented phospholipid micelles as a tool for the study of membrane-associated molecules. *Progress NMR Spectrosc.* 26:421–444.

16. Sanders, C. R., and R. S. Prosser. 1998. Bicelles: a model system for all seasons? *Structure*. 16:1227–1234.

17. Marcotte, I., and M. Auger. 2005. Bicelles as model membranes for solid- and solution-state NMR studies of membrane peptides and proteins. *Concepts Magn. Reson.* 24A:17–37.

18. Sanders, C. R., and J. P. Schwonek. 1992. Characterization of magnetically orientable bilayers in mixtures of dihexanoylphosphatidylcholine and dimyristoylphosphatidylcholine by solid-state NMR. *Biochemistry.* 31:8898–8905.

19. Ram, P., and J. H. Prestegard. 1988. Magnetic field induced ordering of bile salt/phospholipid micelles: new media for NMR structural investigations. *Biochim. Biophys. Acta.* 940:289–294.

20. Nieh, M.-P., C. J. Ginka, S. Krueger, R. S. Prosser, and J. Katsaras. 2001. SANS study of the structural phases of magnetically alignable lanthanide-doped phospholipid mixtures. *Langmuir*. 17:2629–2638.

21. Nieh, M.-P., C. J. Ginka, S. Krueger, R. S. Prosser, and J. Katsaras. 2002. SANS study of the effect of lanthanide ions and charged lipids on the morphology of phospholipid mixtures. *Biophys. J.* 82:2487–2498.

22. Rowe, B. A., and S. L. Neal. 2003. Fluorescence probe study of bicelle structure as a function of temperature: developing a practical bicelle structure model. *Langmuir*. 19:2039–2048.

23. Arnold, A., T. Labrot, R. Otla, and E. J. Dufourc. 2002. Cation modulation of bicelle size and magnetic alignment as revealed by solid-state NMR and electron microscopy. *Biophys. J.* 83:2667–2680.

24. Triba, M. N., D. E. Warschawski, and P. F. Devaux. 2005. Reinvestigation by phosphorus NMR of lipid distribution in bicelles. *Biophys. J.* 88:1887–1901.

25. King, V., M. Parker, and K. P. Howard. 2000. Pegylation of magnetically oriented lipid bilayers. *J. Magn. Reson.* 142:177–182.

26. Johnsson, M., and K. Edwards. 2001. Phase behavior and aggregate structure in mixtures of dioleoylphosphatidylethanolamine and poly(ethylene glycol)-lipids. *Biophys. J.* 80:313–323.

27. Johnsson, M., and K. Edwards. 2003. Liposomes, disks, and spherical micelles: aggregate structure in mixtures of gel phase phosphatidylcholine and poly(ethylene glycol)-phospholipids. *Biophys. J.* 85:3839–3847.

28. Johansson, E., C. Engvall, M. Arfvidsson, P. Lundahl, and K. Edwards. 2005. Development and initial evaluation of PEG-stabilized bilayer disks as novel model membranes. *Biophys. Chem.* 113:183–192.

29. Crowell, K. J., and P. M. Macdonald. 1999. Surface charge response of the phosphatidylcholine headgroup in bilayered micelles from phosphorus and deuterium NMR. *Biochim. Biophys. Acta.* 1416:21–30.

30. Crowell, K. J., and P. M. Macdonald. 2001. Europium III binding and the reorientation of magnetically aligned bicelles: insights from deuterium NMR spectroscopy. *Biophys. J.* 81:255–265.

31. Tanner, J. E. 1970. Use of the stimulated echo in NMR diffusion studies. *J. Chem. Phys.* 52:2523–2526.

32. Fauth, J.-M., A. Schweiger, L. Braunschweiler, J. Forrer, and R. R. Ernst. 1986. Elimination of unwanted echoes and reduction of dead time in three-pulse electron spin-echo spectroscopy. *J. Magn. Reson.* 66:74–85.

33. Gibbs, S. J., and C. S. Johnson. 1991. A PFG NMR experiment for accurate diffusion and flow studies in the presence of eddy currents. *J. Magn. Reson.* 93:395–402.

34. Mills, R. 1973. Self-diffusion in normal and heavy water in the range 1–45°. *J. Phys. Chem.* 77:685–688.

35. Losonczi, J. A., and J. H. Prestegard. 1998. Improved dilute bicelle solutions for high-resolution NMR of biological macromolecules. *J. Biomol. NMR.* 12:447–451.

36. Ottinger, M., and A. Bax. 1998. Characterization of magnetically oriented phospholipid micelles for measurement of dipolar couplings in macromolecules. *J. Biomol. NMR.* 12:361–372.

37. Finer, E. G., A. G. Flook, and H. Hauser. 1972. Mechanism of sonication of aqueous egg yolk lecithin dispersions and nature of the resultant particles. *Biochim. Biophys. Acta.* 260:49–58.

38. Cross, K. J., K. T. Holmes, C. E. Mountford, and P. E. Wright. 1984. Assignment of acyl chain resonances from membranes of mammalian cells by two-dimensional NMR methods. *Biochemistry.* 23:5895–5897.

39. Wästerby, P., G. Orädd, and G. Lindblom. 2002. Anisotropic water diffusion in macroscopically oriented lipid bilayers studied by pulsed magnetic field gradient NMR. *J. Magn. Reson.* 157:156–159.

40. Chung, J., and J. H. Prestegard. 1993. Characterization of field-ordered aqueous liquid crystals by NMR diffusion measurements. *J. Phys. Chem.* 97:9837–9843.

41. Gaemers, S., and A. Bax. 2001. Morphology of three lyotropic liquid crystalline biological NMR media studied by translational diffusion anisotropy. *J. Am. Chem. Soc.* 123:12343–12352.

42. Callaghan, P. T., and O. Söderman. 1983. Examination of the lamellar phase of aerosol OT/water using pulsed field gradient nuclear magnetic resonance. *J. Phys. Chem.* 87:1737–1744.

43. Vold, R. R., and R. S. Prosser. 1996. Magnetically oriented phospholipid bilayered micelles for structural studies of polypeptides. Does the ideal bicelle exist? *J. Magn. Reson. B.* 113:267–271.

44. Gustafsson, J., G. Orädd, G. Lindblom, U. Olsson, and M. Almgren. 1997. A defective swelling lamellar phase. *Langmuir*. 13:852–860.

45. Petersen, N. O., and S. I. Chan. 1977. More on the motional state of lipid bilayer membranes: interpretation of order parameters obtained from nuclear magnetic resonance experiments. *Biochemistry.* 16:2657–2667.

46. Lipari, G., and A. Szabo. 1980. Effect of librational motion on fluorescence depolarization and nuclear magnetic resonance relaxation in macromolecules and membranes. *Biophys. J.* 30:489–506.

47. Brainard, J. R., and A. Szabo. 1981. Theory for nuclear magnetic relaxation of probes in anisotropic systems: application to cholesterol in phospholipid vesicles. *Biochemistry.* 20:4618–4628.

48. Schmidt-Rohr, K., and H. W. Spiess. 1994. Multidimensional Solid-State NMR and Polymers. Academic Press, London, UK.

49. Van Beijeren, H., and R. Kutner. 1985. Mean square displacement of a tracer particle in a hard-core lattice gas. *Phys. Rev. Lett.* 55:238–241.

50. Saxton, M. J. 1987. Lateral diffusion in an archipelago. The effect of mobile obstacles. *Biophys. J.* 52:989–997.

51. Saffman, P. G., and M. Delbrück. 1975. Brownian motion in biological membranes. *Proc. Natl. Acad. Sci. USA.* 72:3111–3113.

52. Vaz, W. L. C., R. M. Clegg, and D. Hallmann. 1985. Translational diffusion of lipids in liquid crystalline phase phosphatidylcholine multilayers. A comparison of experiment with theory. *Biochemistry.* 24:781–786.

53. Montesano, G., R. Bartucci, S. Belsito, D. Marsh, and I. Sportelli. 2001. Lipid membrane expansion and micelle formation by polymer-grafted lipids: scaling with polymer length studied by spin label electron spin resonance. *Biophys. J.* 80:1372–1383.